Coupling Between Mesoplasticity and Damage in High-cycle Fatigue

Laurent Flaceliere, Franck Morel, André Dragon

Coupling Between Mesoplasticity and Damage in High-cycle Fatigue

LAURENT FLACELIERE,[1,*] FRANCK MOREL[2] AND ANDRÉ DRAGON[1]

[1]*E.N.S.M.A., Laboratoire de Mécanique et de Physique des Matériaux (LMPM), UMR 6617, Site du Futuroscope BP 109, 86960 Futuroscope Cedex, France*

[2]*E.N.S.A.M., Laboratoire Procédés Matériaux Instrumentation (LMPI) UMR 1427, 2 Boulevard du Ronceray, BP 93525 49025 Angers Cedex, France*

ABSTRACT: The multiaxial fatigue loading in the high-cycle regime leads to localized mesoscopic plastic strain that occurs in some preferential directions of individual grains for most metallic materials. Crack initiation modeling is difficult in this fatigue regime because the scale where the mechanisms operate is not the engineering scale (macroscopic scale), and local plasticity and damage act simultaneously. This article describes a damage model based on the interaction between mesoplasticity and local damage for the infinite and the finite fatigue life regimes. Several salient effects are accounted for via a simple localization rule, which connects the macroscopic scale with the mesoscopic one, and by the model presented here, which describes the coupled effects of mesoplasticity and damage growth.

Irreversible thermodynamics concepts with internal state variables are used to maintain a balance between extensive descriptions of plastic flow and damage events. Cyclic hardening behavior is described by a combined isotropic and kinematic hardening rule while the damage evolution is governed notably by the accumulated plastic mesoscopic strain. In this study, predictions are compared to fatigue tests performed on a mild steel (C36) under different loading modes. All the experiments are carried out under in-phase loading conditions: reversed tension, torsion, and combined tension–torsion. The mean stress effect is also studied through tests conducted under tension. The predicted Wöhler curves under any loading mode can be readily obtained with this model, but the main feature of this approach is to ensure a clear link between the mesoscopic parameters like the hardening behavior of individual grains and the subsequent local damage.

KEY WORDS: multiaxial fatigue, damage model, mesoplasticity, experiment.

INTRODUCTION

$\mathbf{M}$ANY ATTEMPTS HAVE been made to describe the behavior and the evolution of damage for different kinds of solid materials submitted to high-cycle fatigue (HCF). For this particular fatigue regime, damage can be considered as a process of progressive deterioration of the material, at the mesoscopic scale (Lemaître, 1992). This deterioration should be properly handled from the thermodynamic standpoint, taking into account the irreversibility of the cumulative damage process. This assumes a clear distinction between the plasticity and damage effects on the physically representative scale, and this distinction is made according to the major cause of degradation of material properties (Lemaître, 1992). The two phenomena are, of course, coupled and this feature must be carefully examined.

Continuum damage mechanics considers the concept of 'delocalized' defects, that is defects whose physical presence has not necessarily been confirmed (Chaboche, 1974). This leads to the study of early stage effects with respect to what happens at the end of the life of the sample, even before a dominant macrocrack occurs. The defects concerned could be, for example, microcavities initiated in a 'well-oriented' grain. The detailed position of such defects and their dimensions, do not need to be known, as the material is regarded as being continuous. Hence, the use of the term 'continuum damage mechanics' (CDM).

When dealing with fatigue crack growth, linear elastic fracture mechanics has proved its capacity to reflect the main trends of crack propagation or the advanced part of 'damage'. However, when dealing with microdefects, for example small cracks (i.e., 'small' as compared to the microstructure) or when the crack growth in shear bands is observed, fracture mechanics tools are inadequate. Moreover, the mechanism that results in the appearance and growth of small cracks in shear bands is closely related to plasticity and damage, both of them strongly interacting with each other.

REVIEW OF SELECTED DAMAGE MODELS APPLIED TO HIGH-CYCLE FATIGUE (HCF)

In this section, we will review four different models, based on damage mechanics, which account for some salient phenomena that occur during cyclic loading. The first approach is an early model proposed by Chaboche (1974) and Chaboche and Lesne (1988). It is strongly phenomenological and based on the identification of a differential law to describe damage progression. The second model, suggested by Yang and Chow (2003), presents an interesting compromise between the phenomenological

approach and micromechanical modeling. The third model developed by Lemaître (1992) includes scale transition (from the macroscopic scale to the mesoscopic scale) and an explicit description of the plastic behavior of crystal. Hence, it is able to take into account more complex stress states. The last model presented here is proposed by Hoshide and Socie (1987, 1988) and Socie (1993); it puts forward a propagation point of view on the critical planes.

The HCF Model of Chaboche

The model proposed by Chaboche (1974) has been put forward for metallic materials, and describes the different steps of the fatigue process: accommodation, initiation, and microcrack propagation. The author assumes that the scale of observation is the 'engineering scale', and the loading parameters considered are the maximum macroscopic stress $\Sigma_{\max}$ and the mean macroscopic stress $\overline{\Sigma}$ for each cycle. In order to take into account non-linear damage evolution which occurs for example with block loading (Figure 1), the damage increment $\mathrm{d}D$ is considered to be dependent on the damage D (macroscopic damage variable), for each cycle increment $\mathrm{d}N$.

$$\mathrm{d}D = f\big(\Sigma_{\max}, \overline{\Sigma}, D\big)\,\mathrm{d}N \tag{1}$$

This model is able to reflect damage growth below the fatigue limit of the material once the damage is initiated. It is shown that the fatigue
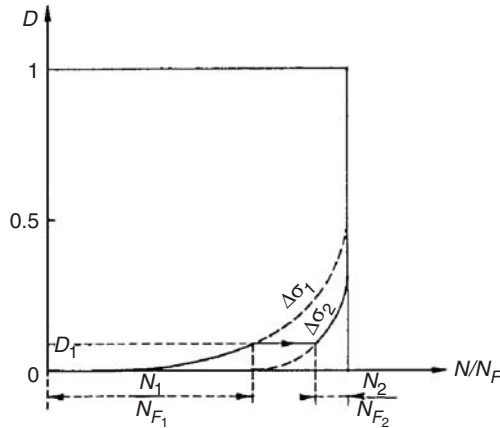

Figure 1. *Non-linear damage accumulation for a two block loading (Chaboche model)* *(Chaboche, 1974).*

limit (damage threshold) is reduced by damage accumulation (Chaboche and Lesne, 1988). This is not necessarily in correlation with experimental results (De Los Rios et al., 1984). This model is one of the first to be devoted to fatigue and built in the framework of CDM. It brings forward non-linear damage evolution, efficient treatment of multiple levels tests (loadings by blocks), and a complete description of the SN curve (stress according to number of applied cycles, with $N = 10–10^7$ cycles). These effects will be included in the model proposed in the present article.

The Viscoplastic Fatigue Damage Model Proposed by Chow and co-workers

This constitutive model by Yang and Chow (2003) and by Wei et al. (2000) captures the response of a complex material subjected to a variety of loading paths including fatigue loadings. The model is based on experimental study, in particular for 63Sn–37Pb solder joints subjected to thermo-mechanical fatigue. Internal state variables are used to characterize temperature effect and material degradation observed. A damage-coupled viscoplastic constitutive model is formulated. Equation (2) allows one to determine explicitly the accumulated equivalent inelastic strain rate $\dot{p}^{in}$, by incorporating different effects embodied by several parameters.

$$\dot{p}^{in} = \frac{1-\mu}{1-D} f \exp\left(\frac{-Q}{RT}\right)\left(\frac{\lambda_0}{\lambda}\right)^p \sin(h^m)\left(\frac{1-\mu}{1-D}\frac{J_2}{(c+\hat{c})}\right) \qquad (2)$$

J_2 is the second invariant of the deviatoric stress, D and μ are damage variables, f, p, m, and Q are material parameters, R is the gas constant, T is the absolute temperature, λ is the current grain (or phase) size, λ_0 is the initial phase size, c and $\hat{c}$ are state variables. It is important to note that all these quantities are defined at the macroscopic scale. This formulation illustrates the evolution of damage, by a competition between the effect of the variables D and μ. The evolution equations for the two damage variables, D and μ, are established within the framework of irreversible thermodynamics

$$\dot{D} = -\dot{\omega}\frac{Y_D}{2Y_d} \qquad (3)$$

where

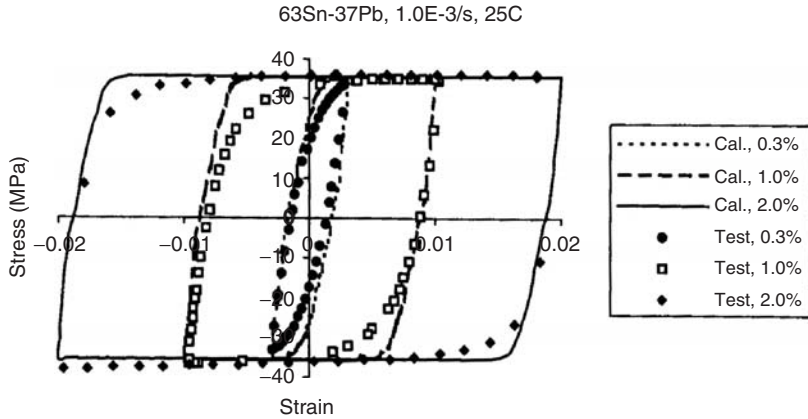$$Y_d = \left[\frac{1}{2}(Y_D^2 + \gamma Y_u^2)\right]^{1/2} \qquad (4)$$

63Sn-37Pb, 1.0E-3/s, 25C

Figure 2. *Hysteresis loops for different strain ranges under strain rate 10^{-3}/s at temperature 25°C (Yang and Chow, 2003).*

is the equivalent damage energy release rate.

$$\dot{\mu} = -\dot{\omega}\frac{\gamma Y_\mu}{2Y_d} \tag{5}$$

where ω is the equivalent overall damage variable and γ is a material constant. Y_D and Y_μ are the damage energy release rates (driving forces) corresponding to damage variables D and μ, and Y_d is the equivalent damage energy release rate combining Y_d and Y_μ.

The major features of this model are as follows: the macroscopic scale is considered (as in Chaboche (1974) and Chaboche and Lesne (1988)) and specific correlations related to cyclic plasticity introduced (see for example, Figure 2). The model is focused on large and unrecoverable plastic strain at the macroscale scale (generalized plasticity in the case of large plastic strains, or the low cycle fatigue (LCF) regime).

The model under consideration (Yang and Chow, 2003; Wei et al., 2004) is able to take into account many phenomena related to the material (size of grains, modification of phases, . . .), and to the applied loads (stress, temperature, . . .). The isotropic hardening driving (thermodynamic) force given later in this article (Equation (15)), coupled with damage process, was introduced in the somewhat analogous form by Yang and Chow (2003) and Wei et al. (2004) in an empirical manner.

The formulation of damage is stimulative (see also Wei et al. (2000)). The effect of the competition between two damage variables, expressed further by two distinct energy release rates, makes it possible to model different mechanisms. However, the correlation between these mechanisms

needs to be interpreted further. This concept, handled in a different way, will be included in the model proposed in this article.

THE TWO-SCALE MODEL PROPOSED BY LEMAÎTRE

Lemaître (1985, 1992) has attempted to extend the framework of CDM to the fatigue field including its multiscale aspect. In HCF in particular, macroscopic plasticity is for the most part negligible, and crack initiation occurs in localized plasticity spots surrounded by a material in elastic range. Two-scale insight is introduced to account for the fact that HCF damage takes place on a smaller scale than the engineering scale (Lemaître, 1985). Consequently, this approach considers a microscopic spherical inclusion within an elasto-plastic damage framework in a macroscopic infinite elastic or eventually elasto-plastic matrix (Figure 3). Damage is then localized on a microscopic scale, with negligible influence on the macroscopic scale. Elastic behavior is assumed to be identical within the inclusion and in the matrix. The introduction of the effective stress concept, initially dedicated to the unidimensional creep process, was the starting point for this model. The stress localization – in the sense of scale transition from the matrix scale to the inclusion scale – is carried out following the analysis of Eshelby (1957), within the framework of the self-consistent models, like the one proposed by Berveiller and Zaoui (1979):

$$\underline{\underline{\sigma}} = \underline{\underline{\Sigma}} - 2\mu(1 - \beta_l)\left(\underline{\underline{\varepsilon}}^p - \underline{\underline{E}}^p\right) \tag{6}$$

where $\underline{\underline{E}}^p$ and $\underline{\underline{\Sigma}}$ are the macroscopic elastic strain and stress tensor, respectively, $\underline{\underline{\varepsilon}}^p$ and $\underline{\underline{\sigma}}$ are the mesoscopic plastic strain and stress tensor, and
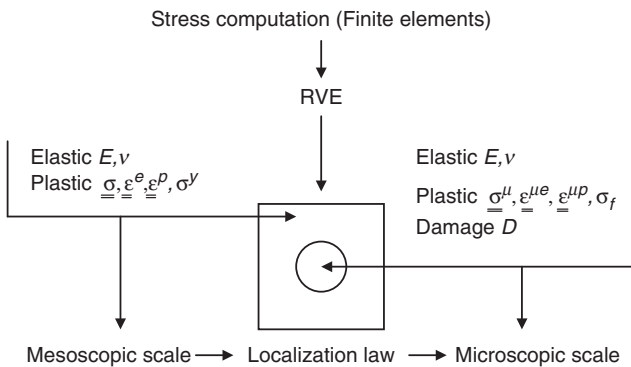

Figure 3. *Lemaître two-scale model.*

the coefficient β_1 depends on the stress ratio. The mechanical degradation of the inclusion, due to the fatigue crack initiation, is taken into account by letting the mechanical strength of this inclusion be considered equal to the fatigue limit of the material σ_f (the mechanical weakness of the matrix is not considered). Figure 4 gives an example of predicted normalized mesoscopic yield stress and predicted damage as a function of the normalized number of cycles in torsion.

The evolution of the local yield stress, due to the influence of the mesocrack at the scale of the inclusion is an interesting feature of this model. The damage evolution occurring in the inclusion induces a modification of the microscopic stress (in the inclusion). However, the effective stress concept used in the model fixes the stress redistribution form. This effect could be induced in a different way by using an enhanced form of a thermodynamic potential and the resulting constitutive equations. In the case of the HCF regime, the damage mechanisms are different from those of creep fatigue, and the physical justification for the use of the isotropic effective stress framework is weak. For this HCF model, the decrease of the damage threshold which occurs as the damage grows is a way to take into account the reduction of the fatigue limit during the sample life.

The model by Lemaître considers the complete lifetime of a specimen (initiation, short-crack growth, and long-crack growth), and hence focuses
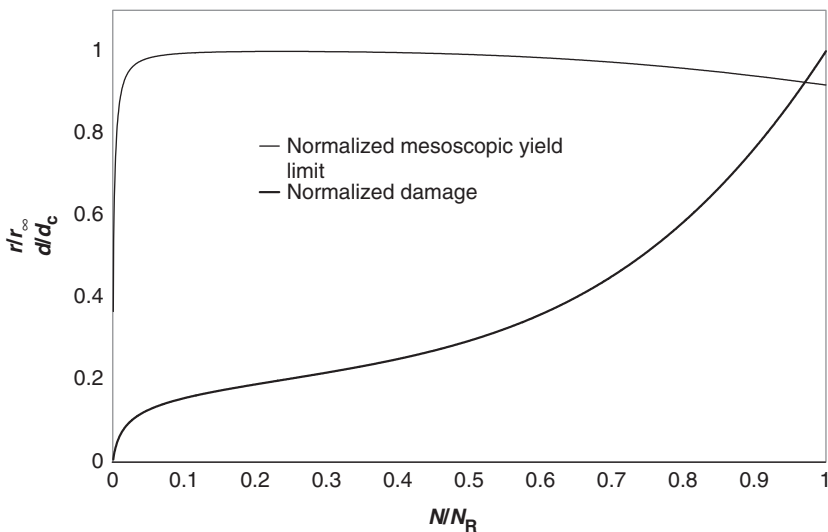

Figure 4. *Normalized mesoscopic yield stress (r/r_∞) and normalized damage (d/d_c) in function of the normalized number of cycles in torsion ($\Gamma_a = 165\,MPa$ that induce number of cycles equal to failure $N_R = 1.7 \times 10^6$ cycles).*

on the macroscopic degradation of the sample. Indeed, numerical calculations show intense damage evolution near failure. This is the consequence of the model taking into account phenomena relevant to fracture mechanics (at the end of the lifetime). The application of the effective stress concept to creep fatigue leads to the analogous effect with a loss of rigidity only at the end of the test immediately before the failure of the specimen. In HCF, a small loss of macroscopic rigidity (the consequence of meso-cracking) may coincide with significant fatigue damage. The model proposed in this study will be further based on an approach in a way similar to Lemaître's model, without employing the effective stress concept, while looking to refine the description of the evolution of damage. However, the same problem of competition will occur with the 'fracture mechanics' point of view during the crack propagation phase of the sample life.

Crack Nucleation and Growth Model Proposed by Socie

The model proposed by Socie (1993) is based on critical planes of crack growth. The SAE1045 steel studied has microstructure and mechanical properties close to the C36 steel used for our study. A dislocation model is applied to compute the nucleation of cracks within individual grains. Finally, the model adopts a framework based on the classical Paris-type propagation laws. For example, a combination of modes I and II is taken into account for the equivalent strain intensity:

$$\Delta K_{eq} = \sqrt{\left(Y_{\mathrm{I}} F \Delta \varepsilon_n \sqrt{\pi c}\right)^2 + \left(Y_{\mathrm{II}} G \Delta \gamma_m \sqrt{\pi c}\right)^2} \qquad (7)$$

where $\Delta \varepsilon_n$ and $\Delta \gamma_m$ are the normal and shear strain amplitudes on the crack growth plane, c is the crack length, and Y_{I} and Y_{II} are geometry factors depending on aspect ratio. Integrating this law leads to an estimate for the crack propagation life N_{p}:

$$N_{\mathrm{p}} = \int_{c_1}^{c_2} \frac{\mathrm{d}c}{A\left(\Delta K_{eq}\right)^m} \qquad (8)$$

To conclude, this empirical model, regarding the propagation rules, is strongly based on observed mechanisms at the mesoscopic scale (grain size). The developments carried out in this study converge in some respects, in particular, by noting the important role of the critical planes.

FEATURES OF DAMAGE PATTERNS IN TENSION AND TORSION

The steel under consideration (C36) is composed of grains of ferrite and of pearlite, the mean grain size being 16 μm for ferrite and 22 μm for pearlite (Figure 5). The mechanical characteristics of this material are shown in Table 1.

After mechanical polishing (with abrasive paper down to a grain size of 6 μm, and finally, polishing with a diamond paste of 1 μ), all samples were tempered at 500°C for 1 h under a vacuum (to reduce residual stresses). All experimental work was conducted at room temperature and pressure in an air environment on a servohydraulic biaxial testing machine (Instron type 1343) operating in force (and torque) control in the frequency range 10–20 Hz.

For all of the observed specimens in tension (seven samples), the importance of the two critical planes related either to maximum shear stress or maximum principal stress is evident. The plane of maximum shear stress corresponds to the first stages of nucleation and the beginning of short-crack growth (stage I, mode II, corresponding to the plane at 45° to the specimen axis), as shown in Figure 6. After this first phase of shear crack growth, the cracks branch toward a plane of maximum normal stress (stage II, mode I,
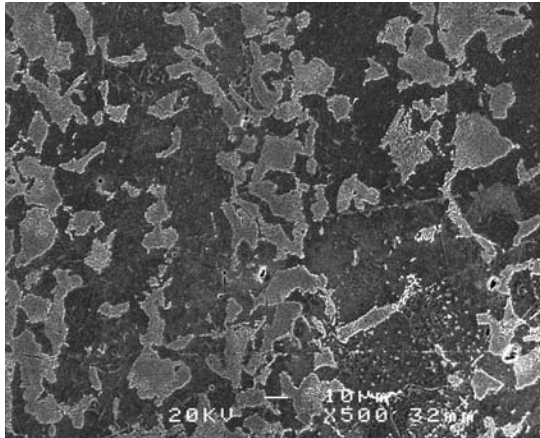

Figure 5. *C36 steel: grains of ferrite (white) and pearlite (black).*

Table 1. *Mechanical characteristics of the C36 steel.*

Young's modulus	$R_{P\,0.2}$ monotonous	$R_{P\,0.2}$ cyclic	R_m	A%
205,000 MPa	350 MPa	280 MPa	580 MPa	30%
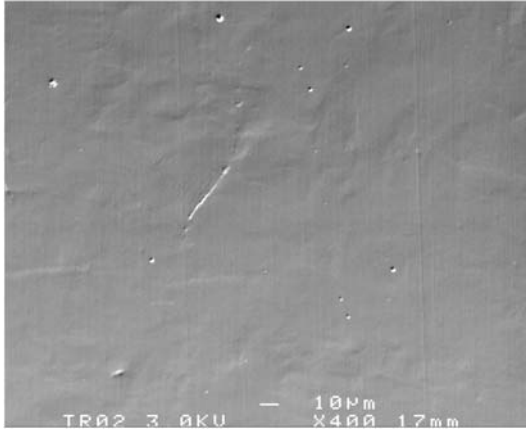
Figure 6. *Tension test-tube after 2×10^5 cycles. Initial observed cracking (number of cycles to failure $= 4.16 \times 10^5$ cycles).*
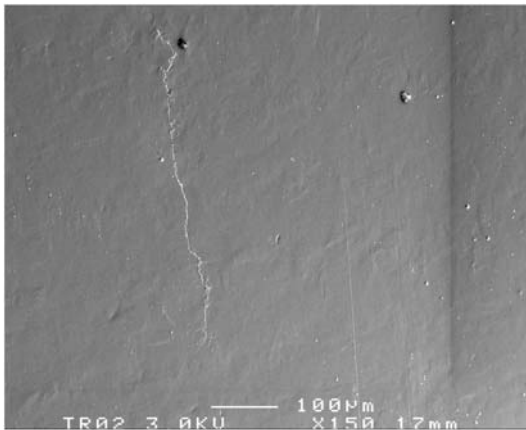

Figure 7. *The same test-tube after 4×10^5 cycles. This crack is the same as in Figure 2 (number of cycles to failure $= 4.16 \times 10^5$ cycles).*

corresponding to the plane normal to the specimen axis) as shown in Figure 7. This branching occurs after a maximum crack length of 20 μm. Observation of the specimen surface shows that the damage is very localized. Very few signs of damage or plasticity are observed elsewhere. All the tension cracks are initiated at either a surface defect (due to polishing), an inclusion (sulfide), or at plastic shear bands occurring at the sample surface.

SEM observations made during the tests clearly show that cracks start to grow after their initiation, but can be stopped by meeting a microstructural barrier such as the pearlite bands. Most of the time, the crack growth speed
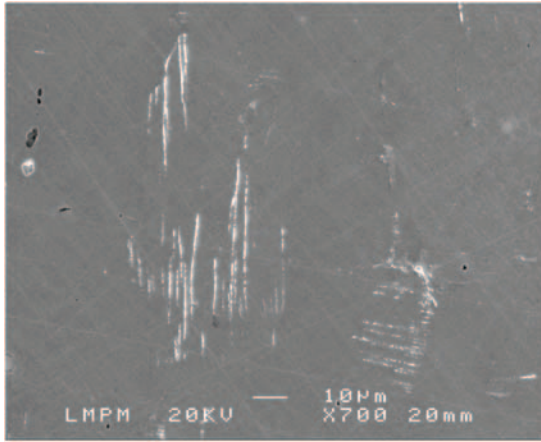
Figure 8. *A torsion test-tube after 10^5 cycles. Accumulative plastic strain on critical mode II planes (number of cycles to failure $= 4 \times 10^5$ cycles).*

increases with the cycling pursued, and finally, a single crack leads to failure. This observation proves that under the corresponding fatigue regime, damage is higly localized and shows that microdamage sites can exhibit growth independently of each other (i.e., growth without interactions).

Under fully reversed torsion loading (five samples), the observations show that the initial first stage of crack initiation is governed by mode II along the planes of maximum shear stress. These planes correspond to the longitudinal and transverse directions relative to the specimen axis. On a specimen where the number of cycles to failure was 8×10^5 cycles, many cracks and plastic shear bands oriented along these two directions, with a length of about $20\,\mu m$ and almost homogenous distribution on the specimen gage length, were observed after 1×10^5 cycles. During the following cycles, new cracks can develop while the existing cracks continue to grow mainly along the longitudinal axis. In the case of the specimen shown in Figure 8, the first crack coalescence is observed after 5×10^5 cycles, at around half of the sample lifetime. This figure clearly illustrates the accumulation of plastic strain in bands. Final failure occurs after the shear crack branches to $45°$ along the plane of maximum normal stress. Figure 9 shows such a crack where stages I and II are clearly distinguished.

In accordance with the observations aforesaid, it is important to point out the different damage mechanisms that exist under pure torsion and pure tension loadings. Tension loadings lead to very few cracks while the damage pattern due to torsion is more diffuse on the specimen surface (Figure 9). The damage kinetics is different, and the damage modeling must correctly reflect this feature.
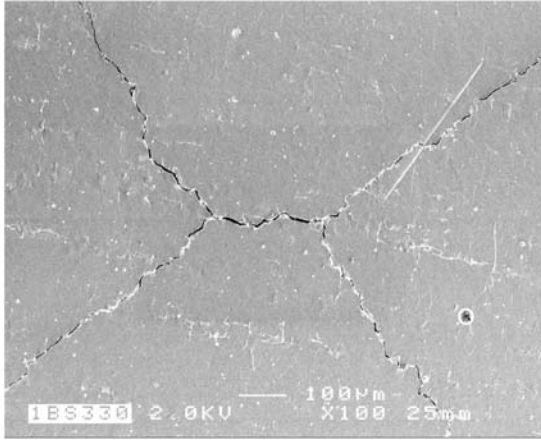
Figure 9. *A torsion test-tube after 8×10^5 cycles near the end of the life of the sample (number of cycles to failure $= 9 \times 10^5$ cycles).*

COUPLED PLASTICITY-DAMAGE MODEL
FOR HCF: NEW PROPOSAL

In the following, a model devoted to the problem of HCF of metallic materials is presented. It is based on a simple micromechanical approach, where plasticity and damage are coupled and expressed at the mesoscopic scale.

The goal of the new proposal is to describe the salient features of the mesoscopic behavior of the crystal (notably plastic strain accumulation in localized grains), using the ideas and postulates put forward in the models previously discussed. These are in particular:

(a) The framework of CDM enabling us to track the damage at each moment in time and for all points of the structure. As stated by McDowell (1999), during the initiation phase, damage can be considered as being homogenous in the representative volume element (RVE).

(b) The choice of meso/micro scale justified by the nature of the physical mechanisms. The transition embodied by a localization rule (macro to meso) allows one to determine the mesoscopic stress and strain from their macroscopic counterparts which are accessible by the engineer.

(c) The mean stress effect accounted for. In particular, it was experimentally shown that the mean shear stress has no effect on the fatigue limit, whereas mean normal stress influences the amplitude of the admissible stress.

(d) It is stipulated that once initiated, the damage can grow even for load levels below the fatigue limit (or the initial damage threshold) and that damage evolution is non-linear and depends on the stress level.

A compromise between the phenomenological approach and a complex multiscale description seems to be appropriate for dealing with the HCF problem. The proposed model considers material evolution at the mesoscopic scale, in particular local plasticity, and is based on a simple micromechanical approach, where plasticity and damage are defined and coupled at the scale of the grains size. To obtain the stress and strain fields at this scale, different rules can be introduced (e.g., the Lin–Taylor or the self-consistent scheme, etc.). For the sake of simplicity (Dang Van, 1993), the Lin–Taylor proposal (9) is utilized:

$$\underline{\sigma} = \underline{\underline{\Sigma}} - 2\mu\underline{\varepsilon}^{\mathrm{p}} \tag{9}$$

where $\underline{\sigma}$ and $\underline{\varepsilon}^{\mathrm{p}}$ represent the stress and plastic strain tensors at the mesoscopic scale and $\underline{\underline{\Sigma}}$ is the macroscopic stress tensor. It is important to note that this localization law considers the material, at both the mesoscopic and macroscopic scales to be purely elasto-plastic, undamaged and isotropic. It is known that, for HCF, damage appears in the form of localized shear bands, in specific directions (Figure 8). Consequently, it would eventually be possible to work specifically on this localization problem, and to modifiy the Lin–Taylor proposal. In particular, the relation employed by Lemaître, in relation to the self-consistent scheme, is a possible alternative way.

The framework of irreversible thermodynamics with internal variables for time-independent, isothermal, and small deformations is used. The model is built by assuming the existence of a thermodynamic potential, namely free energy, as well as the existence of dissipation potentials for evolution laws involving distinct multipliers. A normal dissipation is thus postulated for each mechanism (plasticity, damage), while the evolution laws regarding plasticity are governed by associated rules. This is not the case for damage. The axiom of the local accompanying state (LAS) allows one to put forward a constitutive model based on a finite number of state variables (observable and internal) (Bataille and Kestin, 1975) for the dissipative processes. The choice, *a priori*, of uncoupled dissipations for plasticity and damage makes it easier to distinguish between the mechanisms concerned and the corresponding criteria. This choice leads to local plastic straining before any damage occurs.

In the model brought forward, two distinct scalar internal variables are used to account for the evolution of the mesocracking. The first variable *d* is

called 'the damage effect variable' and makes it possible to account for the reduction of the mechanical strength of the crystal, as well as the reduction of its capacity to accommodate strain in the elastic domain. The second variable β, expresses the degree of cumulated degradation of the crystal, by analogy to the cumulated plastic strain variable p. This choice is similar to the proposal of Cordebois and Sidoroff (1979). Further discrimination between d and β is shown below.

The elastic and inelastic parts of the specific free energy of a grain can be written as follows in Equations (10) and (11).

$$\omega = \rho\psi = \omega^e\left(\underline{\varepsilon}^e\right) + \omega^p\left(\underline{\varepsilon}^p, p, d\right) + \omega^d(d, \beta) \tag{10}$$

$$\omega = \frac{1}{2}\left(\underline{\varepsilon} - \underline{\varepsilon}^p\right) : \underline{\underline{C}} : \left(\underline{\varepsilon} - \underline{\varepsilon}^p\right) + \frac{1}{2}c\underline{\alpha} : \underline{\alpha} + \tilde{r}_\infty p\exp(-sd)$$

$$+ \frac{\tilde{r}_\infty}{g}\exp(-gp)\exp(-sd) + \frac{1}{2}q\beta^2. \tag{11}$$

The intrinsic dissipation, at the level of the grains, is given below by:

$$\Phi = \underline{\sigma} : \dot{\underline{\varepsilon}}^p - \underline{x} : \dot{\underline{\alpha}} - r.\dot{p} + F_d\dot{d} - k\dot{\beta} \geq 0. \tag{12}$$

The expression of intrinsic plastic dissipation is well-known, while the presence of the last two terms, accounts for the damage of the crystal in connection with the two damage variables (d and β). The sign preceding each of these terms depends on the sign affecting each driving (thermo-dynamic) force in Equations (14)–(17) in connection with physical meaning (storage or dissipation of energy). The damage effect variable d thus tends to dissipate energy (creation of a new decohesion surface during mesocracking), whereas the cumulated damage variable β tends to store energy (friction effect on the crack faces).

The elastic behavior is classically defined via the derivation of the free energy (11).

$$\underline{\sigma} = \frac{\partial\omega}{\partial\underline{\varepsilon}^e} = \underline{\underline{C}} : \varepsilon^e. \tag{13}$$

It is important to note that in this model, the damage of the crystal is not taken into account via degradation of elastic moduli; this effect is neglected as in some other models where the primary issue is damage and plasticity coupling. At the same time, as shown below, the elastic limit depends on the crystal damage, via the damage effect variable d. The thermodynamic
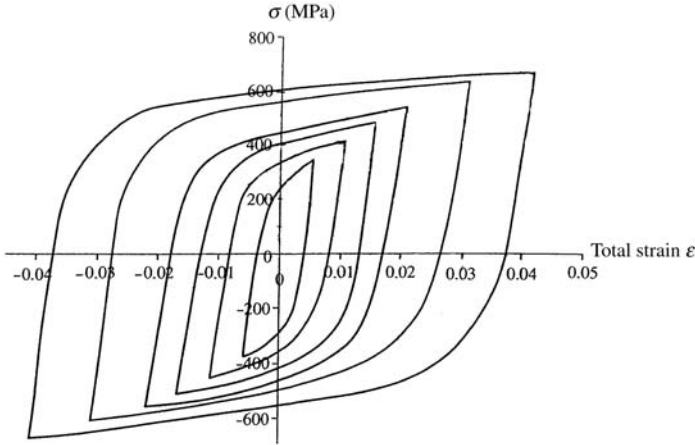
Figure 10. *Stress–strain curves, for the stabilized states, according to several values of total imposed strain (Gros, 1996).*

(conjugate) forces relative to kinematic and isotropic local hardening mechanisms are given as follows:

$$\underset{=}{x} = \frac{\partial \omega}{\partial \underset{=}{\alpha}} = c\underset{=}{\alpha} = c\underset{=}{\varepsilon}^p \tag{14}$$

$$r = \frac{\partial \omega}{\partial p} = r_\infty(1 - \exp(-gp))\exp(-sd). \tag{15}$$

In the last expression, r_∞ designates the saturation value of the driving force r in connection to the yield limit (Equation (18)), g is the hardening parameter and s is a damage sensitivity parameter. This relation incorporates specific coupling effects between plasticity and damage at a local scale. Figure 10 shows the evolution of the yield stress r with the applied number of cycles for pure torsion loading applied to mild steel C36 ($\Sigma_{xy,a} = 165$ MPa). As the damage increases, the degree of isotropic hardening becomes weaker. At the same time, the kinematic hardening, which is not affected by damage, remains active. The isotropic part of the hardening then tends to vanish and a local elastic shakedown state is impossible to reach. Crack initiation and subsequent failure of the component is then likely to occur due to the exhaustion of ductility.

F_d is the conjugate force corresponding to the damage variable d. This force derived from the energy (11) with respect to d depends both on the accumulated plastic strain p and the damage d:

$$F_d = -\frac{\partial \omega}{\partial d} = r_0 + \tilde{r}_\infty s \exp(-sd)\left(p + \frac{\exp(-gp)}{g}\right). \tag{16}$$

A second scalar variable, denoted as β, is defined as the measure of 'cumulated damage'. Its conjugate force is denoted as k and depends linearly on β.

$$k = \frac{\partial \omega}{\partial \beta} = q\beta. \tag{17}$$

The plastic yield condition at the mesoscopic scale is given by (18).

$$f\left(\underline{\underline{\sigma}}, \underline{\underline{x}}, r\right) = J_2\left(\underline{\underline{\sigma}} - \underline{\underline{x}}\right) - (r + r_0) = 0 \tag{18}$$

with

$$J'_2\left(\underline{\underline{\sigma}} - \underline{\underline{x}}\right) = \sqrt{\frac{1}{2}\left(\underline{\underline{s}} - \underline{\underline{x}}\right) : \left(\underline{\underline{s}} - \underline{\underline{x}}\right)} \tag{19}$$

and

$$\underline{\underline{s}} = \underline{\underline{\sigma}} - \frac{1}{3}Tr\left(\underline{\underline{\sigma}}\right) \tag{20}$$

where $\underline{\underline{s}}$ is the mesoscopic stress deviator. The form J'_2 leads to a threshold value equal to the applied shear stress for a pure shear stress and for the first loading increase from 0 ($\underline{\underline{x}} = \underline{\underline{0}}$).

A non-associated law is assumed concerning damage evolution; it stipulates that the damage loading function is distinct from the damage dissipation potential H. Equation (21) gives the damage loading function h, where a is the hydrostatic stress sensitivity coefficient for the damage threshold, and k_0 is the initial damage threshold, while k governs the damage threshold evolution. The function H in (22) shows a similar expression but exhibits a different hydrostatic stress sensitivity parameter b governing the damage growth.

$$h(F_d, k; \sigma_h) = F_d(1 + a\sigma_h) - (k + k_0) \leq 0 \tag{21}$$
$$H(F_d, k; \sigma_h) = F_d(1 + b\sigma_h) - (k + k_1) \tag{22}$$

From the aforesaid assumptions, it is now possible to set the complementary laws, notably the evolution laws for the internal variables of plasticity (23, 24) and damage (25, 26).

$$\underline{\dot{\underline{\alpha}}} = \underline{\dot{\underline{\varepsilon}}}^p = -\dot{\lambda}_p\left(\frac{\partial f}{\partial \underline{\underline{x}}}\right) = \frac{1}{2}\dot{\lambda}_p\frac{\underline{\underline{s}} - \underline{\underline{x}}}{r + r_0} \tag{23}$$

$$\dot{p} = -\dot{\lambda}_p\left(\frac{\partial f}{\partial r}\right) = \dot{\lambda}_p \tag{24}$$

$$\dot{d} = -\dot{\lambda}_p\left(\frac{\partial H}{\partial F_d}\right) = \dot{\lambda}_p(1 + b\sigma_H) \tag{25}$$

$$\dot{\beta} = -\dot{\lambda}_p\left(\frac{\partial H}{\partial k}\right) = \dot{\lambda}_p. \tag{26}$$

This model shows two distinct damage effects: d describes the damage effect on the material properties (see, for example, its influence on the isotropic hardening conjugate force r in (15)), by controlling the change of the elastic surface radius. The second variable, β, is a measure of cumulated damage, by analogy to p in plasticity. The conjugate force to β is k, which represents the damage threshold surface, see also Hayakawa and Murakami (1998). The damage variable β and the damage effect variable d evolve in a convergent or divergent manner depending on the stress-path:

$$\dot{\beta} = \frac{\dot{d}}{(1 + b\sigma_H)}. \tag{27}$$

For a pure torsion loading where the hydrostatic stress is zero, $\dot{\beta} = \dot{d}$.

Finally, all the constitutive equations of this model are summarized in Table 2. It is shown that nine different material constants are required to describe the crystal behavior at the mesoscopic scale. All these parameters are assembled in Table 3, and classified according to their relevance.

Table 2. Constitutive equation of the proposed modeling.

Localization law $\underline{\sigma} = \underline{\Sigma} - 2\mu\underline{\varepsilon}^p$ (9)

Intrinsic free energy (Helmholtz)
$\omega = 1/2(\underline{\varepsilon} - \underline{\varepsilon}^p) : \underline{\underline{C}} : (\underline{\varepsilon} - \underline{\varepsilon}^p) + 1/2c\underline{\alpha} : \underline{\alpha} + \tilde{r}_\infty p \exp(-sd)$
$\quad + (\tilde{r}_\infty)/g \exp(\overline{=}gp)\exp(-sd) + 1/2q\beta^2$ (11)

Mesoplasticity	Damage (non-associated law)
$\underline{\sigma} = \partial\omega/\partial\underline{\varepsilon}^e = \underline{\underline{C}} : \underline{\varepsilon}^e$ (13)	$F_d = -(\partial\omega/\partial d) = r_0 + r_\infty s \exp(-sd)$ $(p + (\exp(-gp))/g)$ (16)
$\underline{x} = \partial\omega/\partial\underline{\alpha} = c\underline{\alpha} = c\underline{\varepsilon}^p$ (14)	$k = \partial\omega/\partial\beta = q\beta$ (17)
$r = \partial\omega/\partial p = r_0$ $\quad + \tilde{r}_\infty(1 - \exp(-gp))\exp(-sd)$ (15)	$h(F_d,k; \sigma_h) = F_d(1 + a\sigma_h) - (k + k_0)$ (21)
$f(\underline{\sigma},\underline{x},r) = J_2(\underline{\sigma} - \underline{x}) - (r + r_0) \leq 0$ (18)	$H(F_d,k; \sigma_h) = F_d(1 + b\sigma_h) - (k + k_1)$ (22)
$\underline{\dot{\varepsilon}}^p = -\dot{\lambda}^p(\partial f/\partial\underline{x}) = 1/2\dot{\lambda}^p(\underline{s} - \underline{x})/(r + r_0)$ (41)	$\dot{d} = \dot{\lambda}^d(\partial H/\partial F_d) = \dot{\lambda}^d(1 + b\sigma_h)$ (25)
$\dot{p} = -\dot{\lambda}^p(\partial f/\partial r) = \dot{\lambda}^p$ (24)	$\dot{\beta} = -\dot{\lambda}^d(\partial H/\partial k) = \dot{\lambda}^d$ (26)

Volume intrinsic dissipation at the mesoscopic scale
$\Phi = \underline{\sigma} : \underline{\dot{\varepsilon}}^p - \underline{x} : \underline{\dot{\alpha}} - r.\dot{p} + F_d\dot{d} - k\dot{\beta} \geq 0$ (12)

Table 3. Mechanical parameters used in the proposed modeling.

Localization rule (elastic parameter)	
μ	Lamé coefficient
Hardening parameters	
c	Kinematic hardening modulus
r_0	Initial yield stress
$r_0 + r_\infty$	Yield stress at saturation
g	Hardening modulus
Damage parameters	
k_0	Initial damage threshold
s	Sensitivity of isotropic hardening to damage
q	Evolution of the damage threshold modulus
a	Effect coefficient of the hydrostatic stress on the damage threshold
b	Effect coefficient of the hydrostatic stress on the damage growth
d_c	Critical value of the damage effect

Plastic and Damage Evolutions, Further Comments

The evolution laws, previously discussed, allow us to establish the plastic strain accumulation and the damage evolution. However, beforehand, it is necessary to establish the plastic multiplier $\dot{\lambda}^p$ and the damage multiplier $\dot{\lambda}^d$ from the respective consistency conditions.

$$\dot{f} = 0 \Rightarrow \frac{\partial f}{\partial \underline{\underline{\sigma}}} : \dot{\underline{\underline{\sigma}}} + \frac{\partial f}{\partial \underline{\underline{x}}} : \dot{\underline{\underline{x}}} + \frac{\partial f}{\partial r} \dot{r} = 0. \tag{28}$$

Introducing (18) into (23) and noting that $(\partial f/\partial \underline{x}) : (\partial f/\partial \underline{x}) = (1/2)$, $(\partial f/\partial r) = -1$, and $\dot{r} = (\partial^2 \omega/\partial p^2)\dot{p} + (\partial^2 \omega/\partial p \partial d)\dot{d}$, it can be seen that:

$$\frac{\partial f}{\partial \underline{\underline{\sigma}}} : \dot{\underline{\underline{\sigma}}} - \frac{1}{2}c\dot{\lambda}^p - \frac{\partial^2 \omega}{\partial p^2}\dot{\lambda}^p - \frac{\partial^2 \omega}{\partial p \partial d}\dot{d} = 0 \tag{29}$$

and finally from (24)

$$\dot{p} = \dot{\lambda}^p = \frac{\left(\partial f/\partial \underline{\underline{\sigma}}\right) : \dot{\underline{\underline{\sigma}}} - (\partial^2 \omega/\partial p \partial d)\dot{d}}{(1/2)c + (\partial^2 \omega/\partial p^2)} \tag{30}$$

$$\frac{\partial \omega}{\partial p \partial d} = -\tilde{r}_\infty s(1 - \exp(-gp))\exp(-sd) \leq 0 \tag{31}$$

where

$$\frac{\partial^2 \omega}{\partial p^2} = \frac{\partial r}{\partial p} = \tilde{r}_\infty g \exp(-gp) \exp(-sd) \tag{32}$$

$$\frac{\partial f}{\partial \underline{\underline{\sigma}}} = \frac{\left(\underline{\underline{s}} - \underline{\underline{x}}\right)}{2J_2'\left(\underline{\underline{s}} - \underline{\underline{x}}\right)}. \tag{33}$$

Equation (30) clearly shows the coupling between plasticity and damage. The evolution of the accumulated plastic strain p is related to the stress path, and to the evolution of the damage effect variable, d.

For the damage consistency, a similar procedure involving $\dot{h} = 0$ leads to the expression of the damage multiplier $\dot{\lambda}^d$, and consequently $\dot{\beta}$ (Equation (26)).

$$\dot{h} = 0 \Rightarrow \frac{\partial h}{\partial F_d}\dot{F}_d + \frac{\partial h}{\partial k}\dot{k} = 0$$

$$\frac{\partial h}{\partial F_d}\dot{F}_d + \frac{\partial h}{\partial k}\frac{\partial k}{\partial \beta}\dot{\beta} = 0 \Rightarrow \dot{\beta} = \dot{\lambda}^d = \frac{-(\partial h/\partial F_d)\dot{F}_d}{(\partial h/\partial k)(\partial k/\partial \beta)}. \tag{34}$$

By noting that $(\partial h/\partial k) = -1$, and by expanding the terms in (34), one obtains:

$$\dot{\beta} = \dot{\lambda}^d = \frac{(1 + a\sigma_H)}{q}\dot{F}_d \tag{35}$$

with

$$\dot{F}_d = -\frac{\partial^2 \omega}{\partial d^2}\dot{d} - \frac{\partial^2 \omega}{\partial d \partial p}\dot{p}. \tag{36}$$

The evolution of the cumulated damage variable β thus depends on the rate of the damage driving force related to the plastic accumulated strain rate $\dot{p}$ (30). The role of the hydrostatic stress is also taken into account by the coefficient a. The damage effect variable rate follows the same construction, with an extra coefficient b occurring in (37).

$$\dot{d} = \frac{(1 + a\sigma_h)(1 + b\sigma_h)}{q}\dot{F}_d. \tag{37}$$

This distinction between the cumulated damage variable β and the damage effect variable d can be explained by considering that β globally corresponds to the storing of energy (dislocation movement and friction of crack faces), whereas d dissipates energy by a decohesion mechanism. These considerations are close to the damage model proposed by Murakami and Kamiya (1997). Moreover, at the end of the seventies, Cordebois and Sidoroff (1979) proposed a damage model for brittle materials based on two different mechanisms. The first mechanism was related to shearing, whereas the second mechanism was assisted by the stress normal to the crack faces. The two different variables accounted for the corresponding effects. It is to be reminded that in the model presented here, the two mechanisms, represented by the two variables, are connected:

$$\dot{\beta} = \frac{\dot{d}}{(1 + b\sigma_H)}. \qquad (27)$$

By using a differential form for the evolution of the damage driving force F_d, it is possible to observe the coupling between the damage effect variable d and the accumulated plastic strain amplitude p (see Equation (39) below), by using the Equations (11), (36), and (38).

$$\frac{\partial^2 \omega}{\partial d^2} = \tilde{r}_\infty s^2 \left(p + \frac{\exp(-gp)}{g} \right) \exp(-sd) \le 0 \qquad (38)$$

$$\dot{F}_d = \frac{q}{(1 + a\sigma_h)(1 + b\sigma_h)} \dot{d} \Rightarrow \left| \begin{array}{l} \dot{d} = \dfrac{-((1 + a\sigma_h)(1 + b\sigma_h)/q)(\partial^2\omega/\partial d\partial p)\dot{p}}{1 + ((1 + a\sigma_h)(1 + b\sigma_h)/q)(\partial^2\omega/\partial d^2)} \\[2ex] \text{with } \dfrac{\partial^2\omega}{\partial d\partial p} \le 0. \end{array} \right. \qquad (39)$$

By substituting (39) into (30), one can derive Equation (40) below, which gives the evolution of p as a function of the stress-path only.

$$\left| \begin{array}{l} \dot{p} = \dfrac{\left(\partial f/\partial \underline{\underline{\sigma}}\right) : \dot{\underline{\underline{\sigma}}}}{A} \\[3ex] \text{with } A = \dfrac{1}{2}c + \dfrac{\partial^2\omega}{\partial p^2} - \left(\dfrac{\partial^2\omega}{\partial p\partial d}\right)^2 \dfrac{(1 + a\sigma_h)(1 + b\sigma_h)}{(\partial k/\partial \beta) + (1 + a\sigma_h)(1 + b\sigma_h)(\partial^2\omega/\partial d^2)}. \end{array} \right. \qquad (40)$$

From (40), it is possible to estimate the local plastic evolutions at any time in the loading cycle. The principal advantage of a non-associated model is the possibility of distinguishing the effects of hydrostatic pressure (first stress invariant) on the damage threshold, damage evolution, and plastic strain evolution, respectively.

The failure of the crystal is defined by a 'critical' value of the damage effect variable d. So, for $d = d_c$, complete failure at the mesoscopic scale of the crystal is assumed. This criterion is built on the damage variable effect d and not on the cumulated damage variable β. This choice corresponds to the significance of these two variables. In fact, the damage effects will produce the failure of specimens, by a degradation of local material properties. This is only possible with the variable d (related to energy dissipation), and not the variable β (energy storage).

It is assumed that the time necessary for the damage transition from the mesoscopic scale to the macroscopic scale is considered to be negligible. This assumption is confirmed by experiments in the HCF regime.

The Role of the Hydrostatic Stress

As previously noted, the spherical part of the stress tensor influences the damage rate laws. Equations (27) and (39) illustrate the consequences of this choice. The hydrostatic stress is regarded as a loading parameter, and not explicitly as an active force. If σ_h had been considered as an active force in expressions (21) and (22) for the functions h and H, the consistency condition applied to the damage threshold function would have contained the term $\dot{\sigma}_h$. This term would have then appeared for the respective evolution laws ($\dot{d}$ and $\dot{\beta}$). The choice of σ_h as a true driving force could be related to particular mechanisms of damage, independently of the stress state. This alternative approach, not developed here, could have important applications, in particular for quasi-brittle materials.

Consequence of the Localization Rule on the Plasticity and Damage Evolution

One of the basic features of this model is the use of stresses and strains defined at the local scale. To describe the transition from macroscopic to mesoscopic scale, a precise localization rule is required. The introduction of the Lin–Taylor transition law assumed in the present context, provides the necessary connection to numerical computations involving the macroscopic stress evolution.

Starting from the expression for the cumulated plastic strain rate, Equation (40), and employing the expression for the plastic multiplier (30), one obtains:

$$\underline{\dot{\varepsilon}}^p = -\dot{\lambda}^p\left(\frac{\partial f}{\partial \underline{x}}\right) = \frac{\left(\partial f/\partial \underline{\sigma}\right) : \underline{\dot{\sigma}}}{A}\frac{(\underline{s}-\underline{x})}{r+r_0} = \frac{(1/2)\left((\underline{s}-\underline{x})/r+r_0\right) : \underline{\dot{\sigma}}}{A}\frac{1}{2}\frac{(\underline{s}-\underline{x})}{r+r_0}.$$

(41)

In the case of proportional loading (and only in this case), the tensors $(\underline{s} - \underline{x})$ and $\underline{\dot{s}}$ are deviatoric and colinear; it can be shown (Dang Van, 1993) that:

$$\left[(\underline{s}-\underline{x}):\underline{\dot{s}}\right](\underline{s}-\underline{x}) = \left[(\underline{s}-\underline{x}):(\underline{s}-\underline{x})\right]\underline{\dot{s}}$$

(42)

$$\underline{\dot{\varepsilon}}^p = \frac{1}{2}\frac{\underline{\dot{s}}}{A}.$$

(43)

In order to find $\underline{S}$, the deviatoric macroscopic stress tensor, the localization rule (9) is introduced into the local plastic strain rate expression:

$$\underline{\dot{\varepsilon}}^p = \frac{1}{2A}\left(\underline{\dot{S}} - 2\mu\underline{\dot{\varepsilon}}^p\right) \Rightarrow \underline{\dot{\varepsilon}}^p = \frac{(1/2)\underline{\dot{S}}}{A+\mu}.$$

(44)

This relation illustrates the role of the localization law, through the sum $A + \mu$ in the denominator. Recall that A is not a constant coefficient but depends on p, d, and σ_h. By using an alternative localization rule, for example by replacing μ by $\mu(1-\gamma)$ to get an alternative self-consistent scheme approximation, the plastic (and consequently the damage) evolution changes but the numerical computation principle remains unchanged. A modification would be to introduce a dependence of the coefficient $\mu(d)$ on damage, as put forward by Sauzay (2000). In this case, the quantity d plays the role of a 'loading' parameter, at least with respect to the localization relation. In the same way, $\dot{p}$ can be expressed as a function of $\underline{\dot{S}}$.

$$\dot{p} = \frac{\sqrt{\underline{\dot{S}}:\underline{\dot{S}}}}{2(A+\mu)}.$$

(45)

Equation (45) gives the accumulated plastic strain rate as a function of macroscopic stress rate. Even if the macroscopic stress deviator rate $\underline{\dot{S}}$

appears explicitly in this equation, one should not forget that A depends on the macroscopic hydrostatic stress. For the selected localization rule, this hydrostatic stress is completely transmitted from the macroscopic scale to the mesoscopic scale, and then no modification of A with the localization is necessary. With other types of localization, the transmission of the hydrostatic stress should be checked.

MATERIAL, IDENTIFICATION PROCEDURE, AND MODEL PREDICTIONS

In the experimental part of this work, a mild steel C36 was subjected to different loading conditions. A part of the experimental results has been used to identify the 11 parameters used by the model (Table 3). The remaining experimental data are used to check the accuracy of the predictions made by the model. The identification procedure discussed below employs only data obtained from uniaxial tension and torsion tests. It should be noted that other identification strategies could be considered, for example, by exploiting the results of multiaxial tests.

Firstly, five elastic–plastic parameters are required to account for the cyclic hardening behavior at the mesoscopic scale: c (kinematic hardening coefficient), g (isotropic hardening coefficient), $r_0 + r_\infty$ (asymptotic yield stress close to the torsion fatigue limit), r_0 (initial yield stress), and μ (Lamé coefficient). The value of this last parameter is asummed to be equal to the typical value for this type of steel ($\mu = 70\,\text{GPa}$). The kinematic hardening coefficient c was identified by using cyclic hardening curves established by Gros (1996), for the same C36 steel. Figure 10 shows these curves, for total imposed strain value varying from 0.5 to 4%, and for various stabilized states. These curves were obtained by the progressive increase of the total imposed strain value (this method gives $c = 2000\,\text{MPa}$).

After the identification of the kinematic hardening coefficient, three parameters related to the plasticity of the crystal must be determined. According to the Von Mises equivalent stress chosen, the saturation yield ($r = r_0 + r_\infty$) is equal to the torsional fatigue limit. (This loading accounts for the maximum elastic shakedown of the crystal for a pure shear stress state.) Moreover, this stress state does not include hydrostatic stress; hence it is possible to eliminate the parameters related to the spherical part of stress tensor. For these two reasons, the identification procedure begins with the use of torsional data. The fatigue limit in torsion for C36 steel is estimated to be $169\,\text{MPa}$ for 10^6 cycles (by using the staircase method $r_0 + r_\infty = 169\,\text{MPa}$). The initial yield r_0, is identified by comparing the expression of plastic dissipation for the present model and the

Taylor expression of plastic work converted to heat for the material under consideration. The corresponding numerical simulations allow one to delimit the value of r_0 (Flaceliere, 2004).

The parameter g controls the effect of cyclic hardening for the crystal, due to the accumulated plastic strain. Its value is selected so that the isotropic hardening threshold reaches the saturated state for cumulated plastic strain values equal to a few percent ($g = 0.1$).

Secondly, three coefficients govern the damage evolution: s reflects the damage influence on the isotropic hardening behavior while q and d_c influence the critical damage at the end of the sample life. The large number of parameters used in this model implies that one parameter must be assumed during the identification procedure (one freedom degree). Consequently, it is necessary to fix one parameter in order to determine all the other parameters from the experimental data. Our choice of the first fixed parameter concerns d_c ($d_c = 3$). Moreover, it is assumed, as Lemaître shows in his two-scale model (Lemaître, 1992), that a reduction in the crystal shakedown capacity of about 30% happens just before the end of the lifetime. Equation (15) then allows us to estimate the order of magnitude of the coefficient of sensitivity to the damage ($s = 0.06$).

The threshold value of damage initiation, k_0, is selected to predict damage activation for lifetime fractions close to that observed in the experiments with torsional loads. This stage corresponds to the formation of local plastic strain in the form of bands, considered as incipient damage ($k_0 = 80$ MPa).

The coefficient of damage shakedown q was obtained by inverse identification (i.e., adjustment on lifetimes obtained in pure torsion tests). In particular, this parameter controls the damage progression ($q = 400$ MPa).

After this first stage of identification, it is possible to plot a 'correlated' Wöhler curve in torsion (Figure 11), together with the experimental fatigue data used in the identification process. It should be noted that this diagram does not constitute a prediction. In such a case do not use ''predicted'' in captions (Figures 11 and 12). The analogous curve representing the tension fatigue Wöhler curve is given in Figure 12.

In torsion, Figures 13 and 14 show the evolution of the damage effect variable and of the mesoscopic yield limit, respectively, as a function of the number of cycles. Three stress amplitudes are considered: $\Gamma_a = 165$, $\Gamma_a = 170$, and $\Gamma_a = 190$ MPa leading to the predicted lives of 1.7×10^6, 7.94×10^5, and 3.2×10^5 cycles. For these torsional loadings, with no hydrostatic stress, the relation $\beta = d$ (27) is verified for the whole process.

The graphs mentioned show an almost linear damage evolution for the stress level $\Gamma_a = 190$ MPa. The corresponding slope increases with an increasing stress amplitude. In HCF, this has been corroborated by the
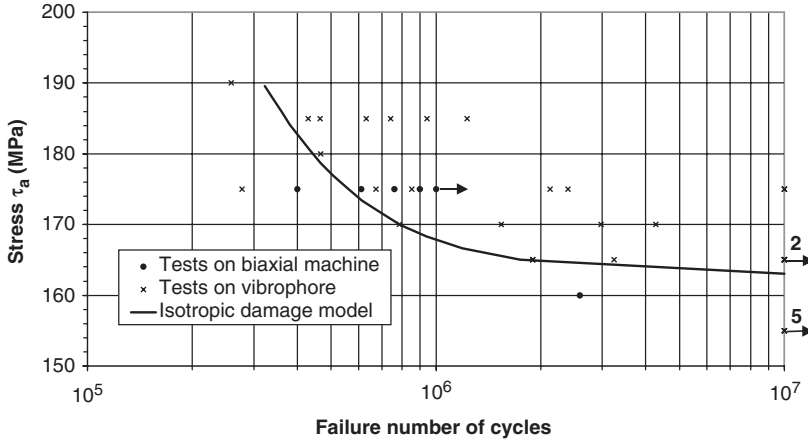
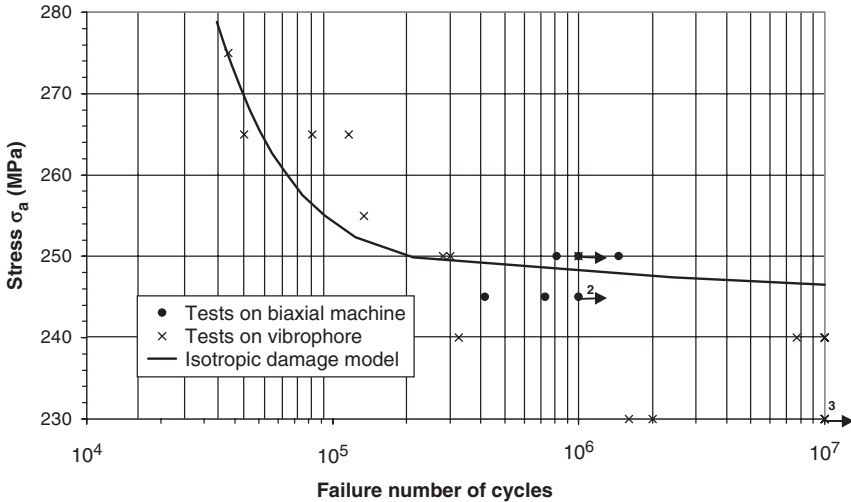**Figure 11.** *Experimental data and corresponding Wöhler curves in torsion.*

Figure 12. *Experimental data and corresponding Wöhler curves in tension.*

observations of Miller (1993). The nucleation phase is shortened, leading to a larger part of the lifetime for damage growth. As shown in Figure 13, the non-linearity increases with a decrease of the stress level. This trend is a direct consequence of the mesoscopic yield limit evolution depicted in Figure 14.

The second step of the identification process takes into account the influence of the hydrostatic stress, which is reflected through the two parameters a and b. Parameter a occurs in the damage threshold
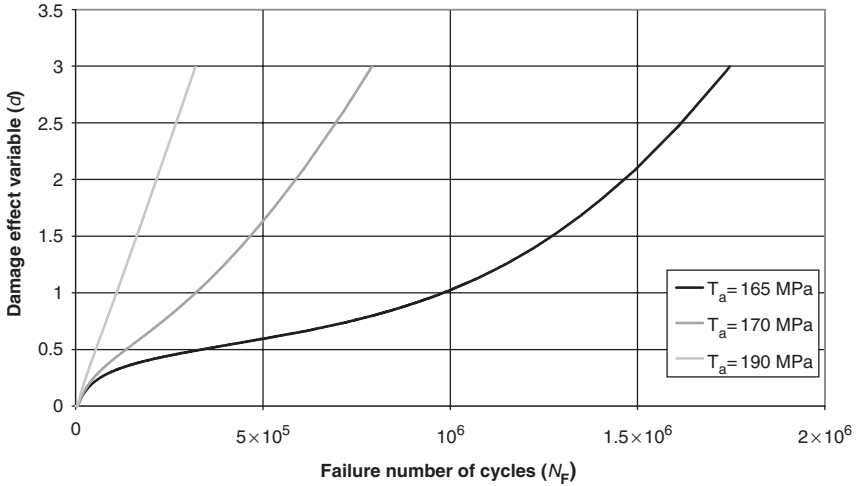
Figure 13. *Predicted damage effect variable d evolutions for three different torsion stress levels.*
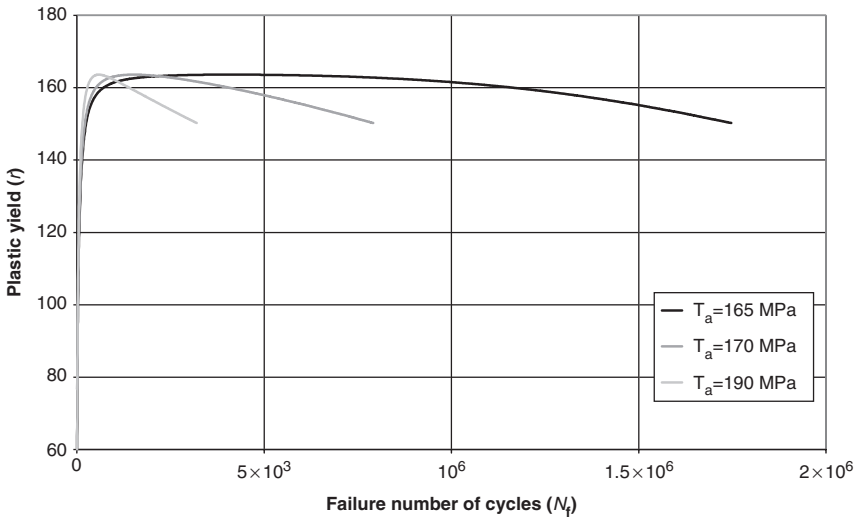

Figure 14. *Predicted mesoscopic yield limit r for three different torsion stress levels.*

whereas b affects damage evolution. The tension fatigue limit and the corresponding SN curve lead to $a = 0.01$ and $b = 0.04$. Table 4 summarizes the values identified for all parameters of the proposed model for C36 steel.

Table 4. Parameters identified for the C36 steel.

C	μ	r_∞	r_0	g	s	k_0	q	d_c
2000 MPa	70 GPa	108 MPa	60 MPa	0.1	0.06	80 MPa	400	3
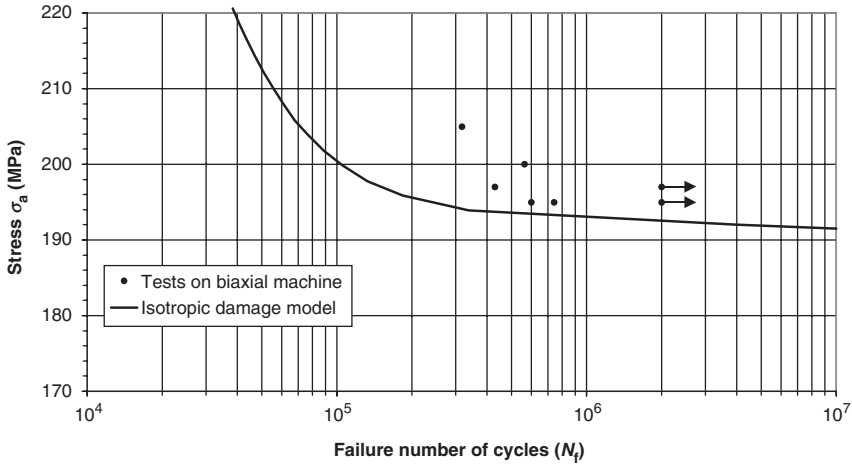
Figure 15. *Tension–torsion (for k=0.5) tests results and predicted Wöhler curve.*

In order to show the predictive capacities of the model, the comparison of the model with fatigue tests carried out under constant amplitude multiaxial conditions has been undertaken. More precisely, results from tests under combined tension and torsion with two stress ratios $k = \tau_a/\sigma_a$ are presented ($k=0.5$ in Figure 15 and $k=1$ in Figure 16). All comparisons shown further in Figure 17 correspond to the fatigue strength for a fatigue life of 10^6 cycles. For the sake of clarity, the experimental points and the calculated data are assembled on the same graph that represents a threshold endurance curve (at 10^6 cycles and for a 50% failure probability) in the plane ($J'_{2,\max}, \Sigma_{H,\max}$). The predicted curve is almost a straight line for positive hydrostatic stresses and all the experimental points lie very close to this line.

It is to be stressed that this curve shows predictive capacities of the model, and not just a simple correlation (Figures 11 and 12), since the identification procedure used only the experimental results obtained in pure tension and in pure torsion, while more complex loading programmes such as combined tension and torsion are exploited in order to validate the model.

When remaining under the macroscopic plastic yield limit in a Haigh diagram (the dotted line in Figure 18), the proposed model provides
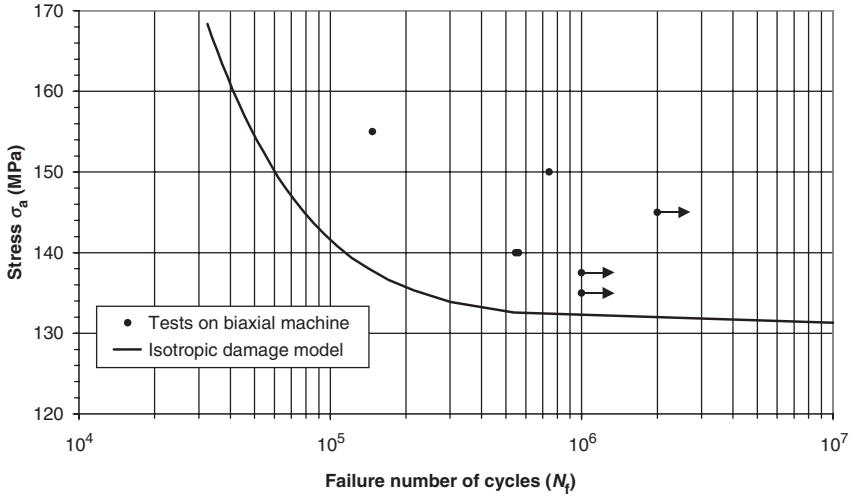
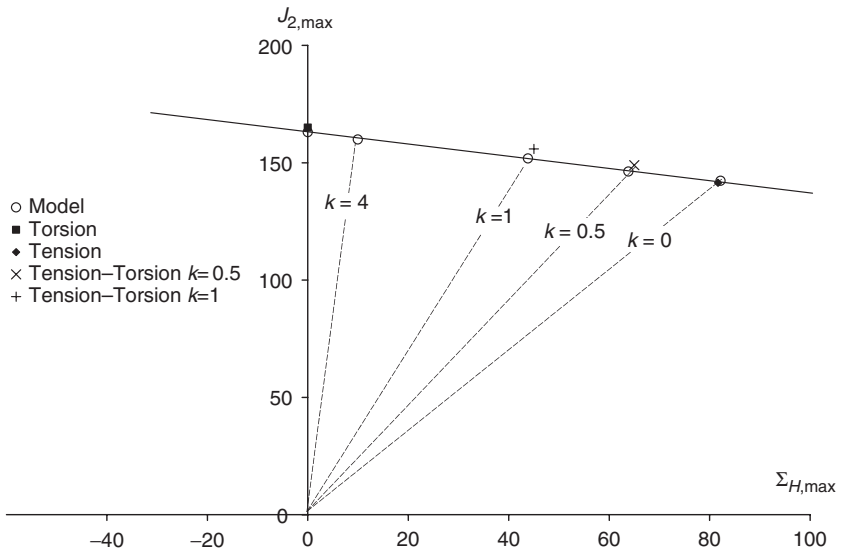**Figure 16.** *Tension–torsion (for k = 1) tests results and predicted Wöhler curve.*

Figure 17. *Predicted threshold endurance curve (at 10^6 cycles and for a 50% failure probability) and experimental data in the plane ($J'_{2,max}, \Sigma_{H,max}$).*

predictions very close to the Gerber curve drawn for endurance limits at 10^6 cycles and to tension data with a load ratio $R = -0.3$. The model presented in this article, therefore, reflects the mean stress effect under tension loads. Let us recall that for a torsional load with a mean level
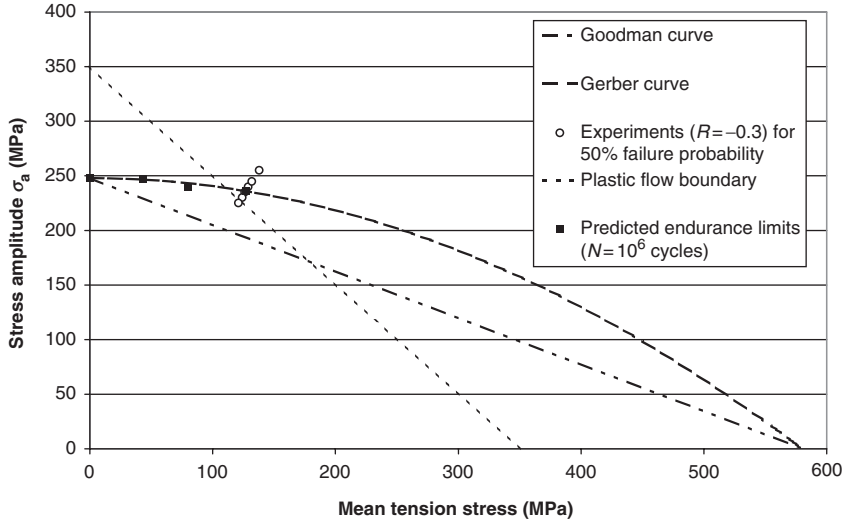
Figure 18. *Goodman and Gerber curves, tests points (R = −0.3) and plastic flow threshold.*

(e.g., $R = \sigma_{zy,\min}/\sigma_{zy,\max} = -0.3$), the model predicts no influence of the mean shear stress on the fatigue strength (Davoli, 2003).

INFLUENCE OF MATERIAL CONSTANTS ON MODEL PERFORMANCE

This section summarizes the influence of the important material constants on the model. This appears useful to illustrate the coupling effects between plasticity and damage, and also to clarify their respective roles. The coefficients were identified for a mild steel (C36), as discussed before.

The first two constants discussed are Lamé's coefficient μ and the kinematic hardening modulus c, occurring in the denominator of the plastic strain rate, Equation (44). The terms derived from the free energy (11) are numerically smaller (second-order significance) compared to the coefficient c. Consequently, the quantities μ and c control the plastic strain accumulation rate. However, μ is much greater than c; hence, μ has a greater influence.

The initial yield stress of the crystal is denoted as r_0. In the first hardening phase, the accumulated plastic strain p increases when r_0 decreases. In particular, r_0 reflects an initial hardening level of the crystal.

The value r_∞ determines the mesoscopic saturation yield stress (15) and the quantity $r = r_0 + r_\infty$ is close to the macroscopic shear fatigue limit of the crystal. Indeed, when the equivalent load level is lower than $r_0 + r_\infty$, there is
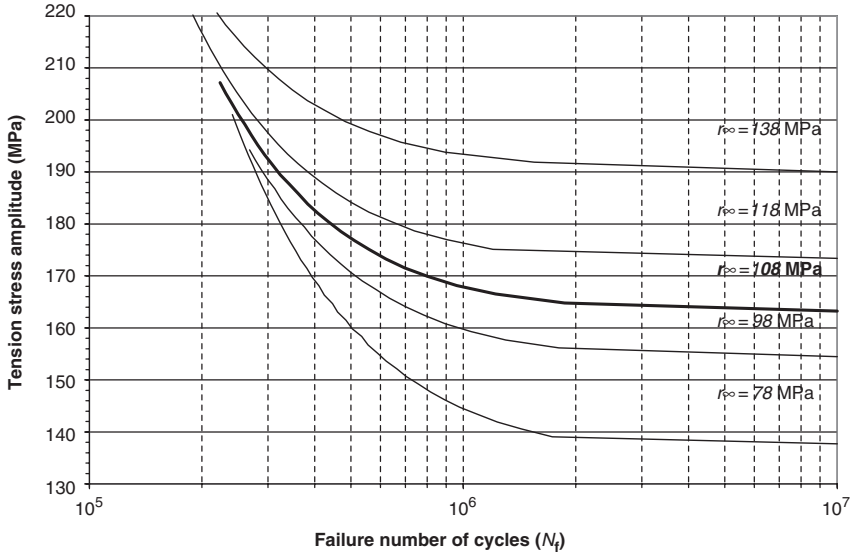
Figure 19. Effect of r_∞ (yield stress at saturation) on the SN curve in pure torsion loading.

an elastic shakedown, with no damage evolution. Figures 19 and 20 illustrate the effect of varying r_∞ on the shape of the SN curves, in tension and in torsion, respectively.

On these Wöhler curves, and on the following ones, it is possible to see that the predictions of the model were extended up to lifetimes of 10^7 cycles. The model proposed and the experimental results and observations are more specifically dedicated to the lifetimes between 10^5 and 10^6 cycles. For this reason, the model predicts flattened forms of the Wöhler curves between 10^6 and 10^7 cycles. Other physical mechanisms, however, will be activated for such lifetimes; they are not considered in this modeling.

The other hardening parameter, g, influences the isotropic threshold evolution r through the plastic strain accumulation p (see also Equation (15)). The greater the g, the more quickly does r tend toward the saturation value $r_0 + r_\infty$. The consequence of a large g value, illustrated in Figure 21, is that the accumulated plastic deformation becomes a quasi-linear function of the number of cycles. The end of a specimen's life is mainly controlled by damage, which induces slope variations with a smaller dependence on the parameter g.

Concerning the parameters related to damage, one can obtain from Equation (16) the initial value of the damage driving force F_d, as given below. The initial value of F_d is not zero, but according to the terminology of Maugin (1999) the 'constrained equilibrum' framework is assumed here in
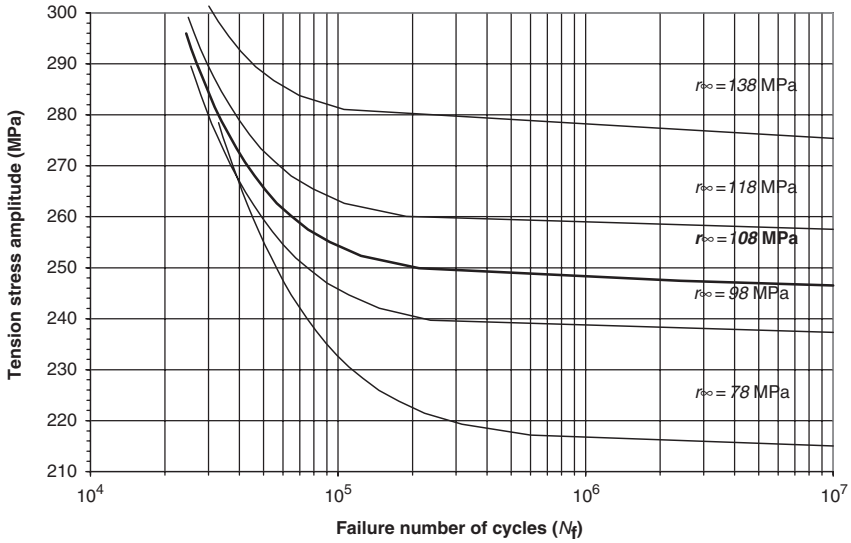
Figure 20. Effect of r_∞ (yield stress at saturation) on the SN curve in pure tension loading.
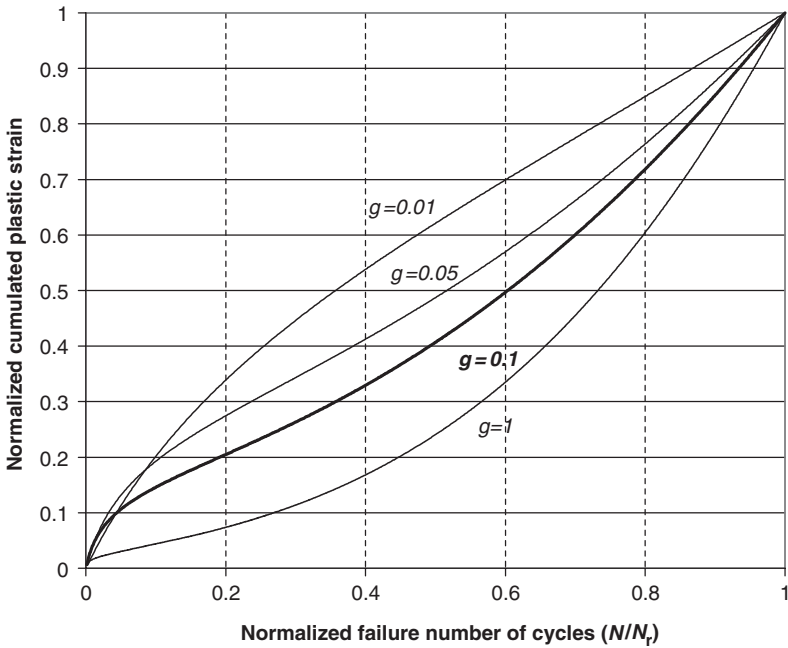

Figure 21. Effect of different values of g (hardening modulus) on predicted cumulated plastic strain in pure torsion loading.
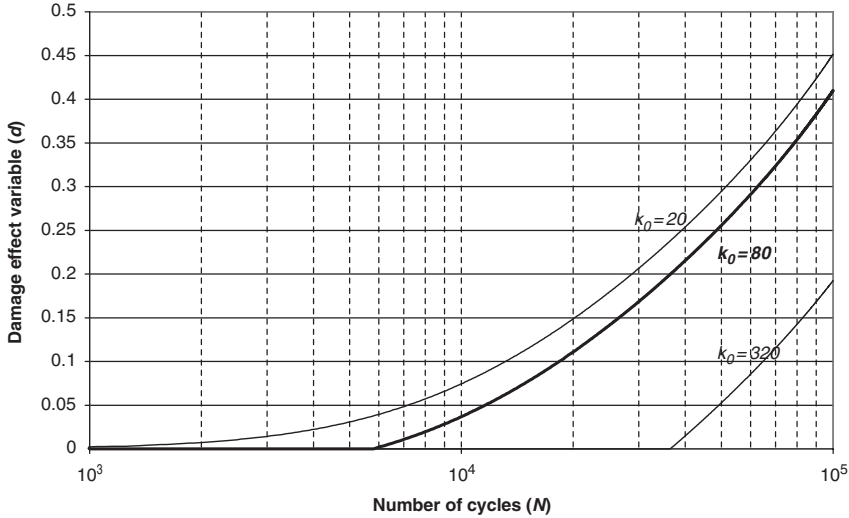
Figure 22. *Effect of k_0 (initial damage threshold) on damage effect variable growth in pure torsion loading.*

relation to the threshold value k_0 regarding the activation of damage. It is thus stipulated that a finite supply of energy is necessary to activate the damage process.

$$F_d(p = 0 \text{ and } d = 0) = \frac{r_\infty s}{g}. \tag{46}$$

Figure 22 illustrates the damage activation conditions as a function of the number of cycles for pure reversed torsion. This effect is similar in tension.

The parameter s is the damage sensitivity coefficient, which for the damage evolution plays the same analogous role as the parameter g does for plastic hardening. Constant s also influences the isotropic hardening yield decrease with respect to damage variable d, see Equation (15). Increasing s increases the damage rate, and makes the fatigue life shorter (Figure 23). The parameter q explicitly controls the damage growth rate, as shown in Equations (37) and (39) (Figure 24).

The critical damage value d_c shifts the SN curve to the left or right side of the SN plane, depending on whether d_c is small or large. Figure 25 gives the effect of d_c on the mesoscopic yield limit evolution in pure torsion. The crack-induced failure ($d = d_c$) puts an end to the yield limit evolution sooner or later depending on the d_c value.
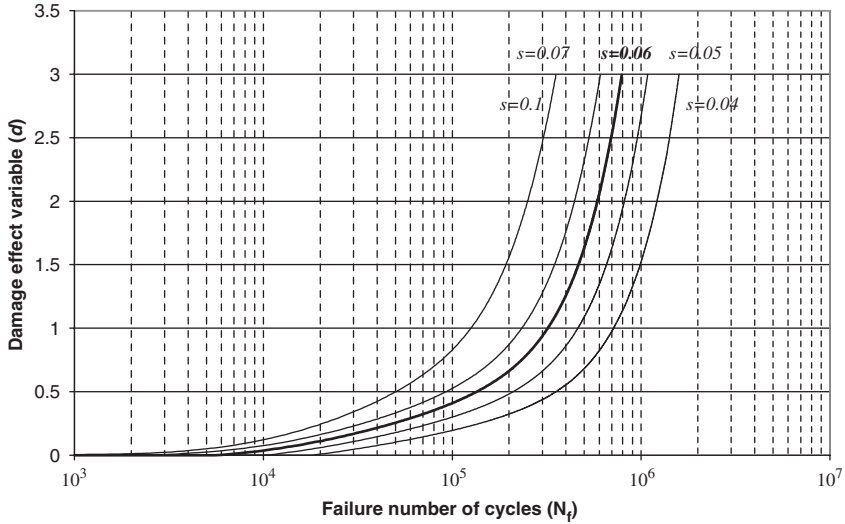
Figure 23. *Effect of s (sensitivity of isotropic hardening to damage) on damage effect variable growth in pure torsion loading.*
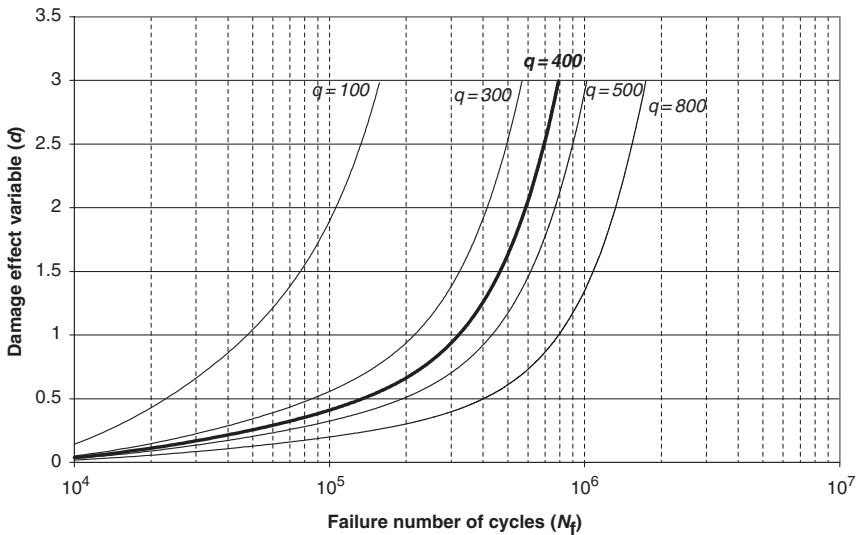

Figure 24. *Effect of q (evolution of the damage threshold) on damage effect variable growth in pure torsion loading.*
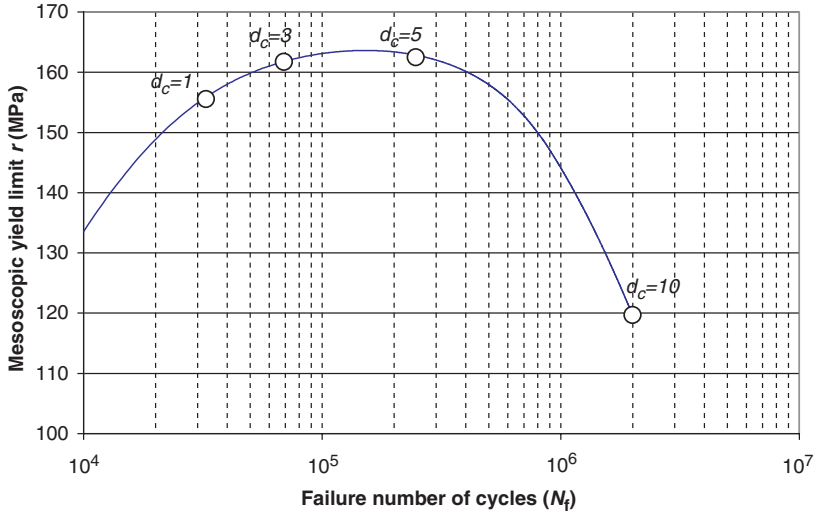
Figure 25. Effect of d_c (critical damage) on the mesoscopic yield limit evolution in pure torsion loading ($\Gamma_a = 170\,MPa$).

The parameters a and b act, respectively, on the damage threshold function and on the damage growth rate, via the hydrostatic stress effect. This implies that there is no influence of these two parameters for a purely deviatoric loading (torsion). This property is used for the identification of the model parameters. Figure 26 shows the effect of a on the tension Wöhler curve. In addition to its influence on fatigue lives, this parameter also controls the fatigue limit level. This is the consequence of the damage activation, depending on the hydrostatic stress affecting the threshold function (21).

Figure 27 illustrates the effect of coefficient b on the evolution of the damage variable d, for pure tension ($\Sigma_{xx,a} = 260\,MPa$, with constant value of a). The slopes of these curves depend on coefficient b. The case where $a = 0.1$ and $b = 1$ is a counterexample where the damage growth appears to be too strong, inducing a knee in the curve.

DISCUSSION AND CONCLUSION

A framework of irreversible thermodynamics with internal variables is employed to put forward a plasticity/damage model applied to multiaxial HCF. Local (mesoscale) plasticity plays a fundamental role in this fatigue regime, and simple mesoscopic cyclic hardening rules are postulated to reflect this feature in the present model. The model leads to the prediction of the fatigue limit (defined as the stress under which no initiation occurs)
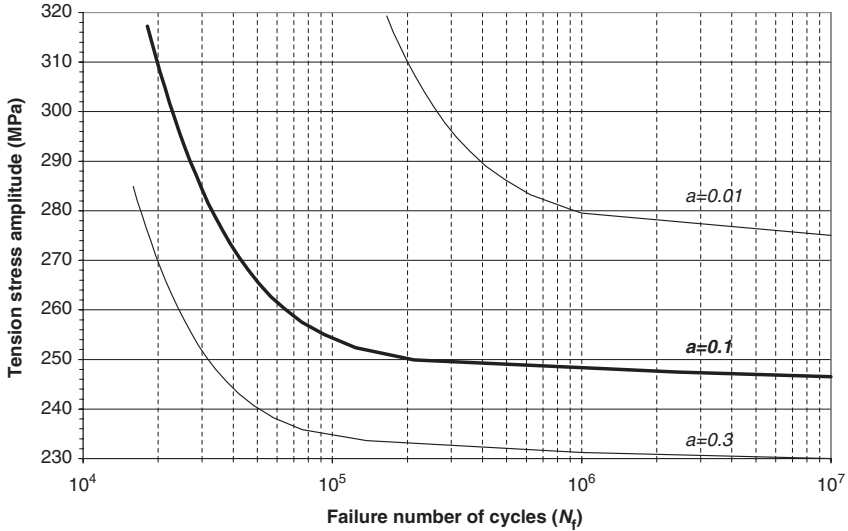
Figure 26. *Effect of the constant a (influence of the hydrostatic stress on the threshold function h) on the SN curves in pure tension loading (b = 0.04 for all curves).*
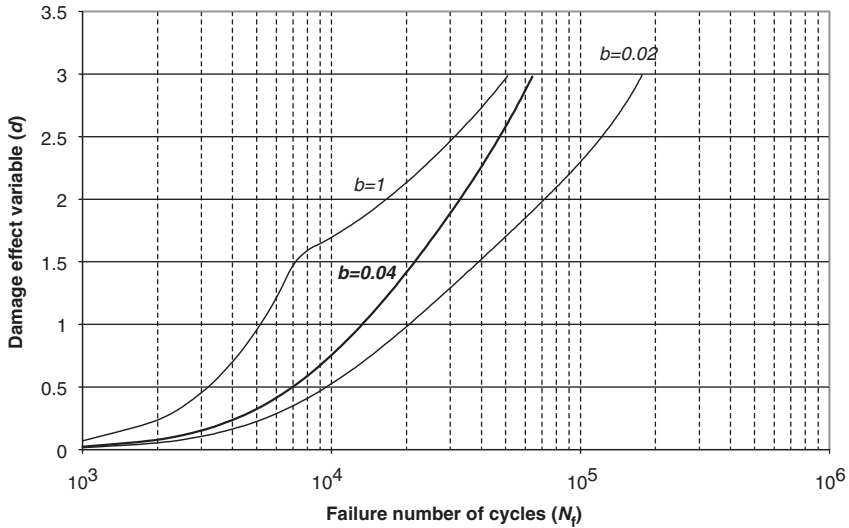

Figure 27. *Effect of the constant b (influence of the hydrostatic stress on the potential function H) on damage effect variable growth in pure tension loading (a = 0.1 for all curves).*

in accordance with the concept of elastic shakedown. It is also able to predict cyclic behavior similar to plastic shakedown because of the coupling between plasticity and damage. Indeed, when a threshold value of the accumulated plastic strain has been reached, damage inhibits yield stress evolution so that only the kinematic part of the hardening remains active. This hardening feature is precisely a condition of plastic shakedown.

Moreover, with this approach, damage nucleation and growth are governed by non-associated law. The effect of the hydrostatic stress on the damage threshold is different to its influence on damage growth. This property is very interesting and none of the classical damage rules applied in HCF make this distinction.

The question of the legitimate application of CDM to deal with the cracks initiation and propagation problem remains open. Depending on the stress state, experimental observations showed that the physical damage of the crystal takes different forms, more or less evenly distributed. In pure torsion, a large quantity and an even distribution of accumulated strain and damage at the sample surface justifies the type of model presented here. However, in tension, the use of a propagation law, as used by Hoshide and Socie (1988), can be legitimate.

When compared to constant amplitude multiaxial fatigue data for mild steel C36, the model predictions are satisfactory. However, it is hoped that further predictive capacities of the model will be demonstrated when it is applied to highly complex loading conditions, including multiaxial stress states and variable amplitude loading conditions.

Fatigue tests based on the regular alternation of multiaxial loading blocks, such as for example tension followed by torsion and vice versa, with changes every 10^5 cycles, for experimental lifetimes limited to 10^6 cycles, have already been carried out. This type of sequence is of particular relevance to the damage accumulation predictions by the model. A forthcoming article will present comparisons between the predictions made by the proposed model and the experimental observations for this type of loading. Further, more complex loading sequences could also be considered in the future (variable amplitude loading, out of phase loading, etc.). An additional coupling with a probabilistic approach could be developed, to account for the significant scatter in fatigue crack growth data.

REFERENCES

Bataille, J. and Kestin, J. (1975). L'interprétation physique de la thermodynamique rationnelle, *Journal de Mécanique*, **14**(2): 365–384.

Berveiller, M. and Zaoui, A. (1979). An Extension of the Self-consistent Scheme to Plastically Flowing Polycrystals, *J. Mech. Phys. Solids*, **26**: 325–344.

Chaboche, J.L. (1974). Une loi différentielle d'endommagement de fatigue avec cumulation non-linéaire, *Rev. Fr. Méc.*, **50–51**: 71–82.

Chaboche, J.L. and Lesne, P.M. (1988). A Non-linear Continous Fatigue Damage Model, *Fatigue Fract. Engng. Mater. Struct.*, **11**(1): 1–17.

Cordebois, J.P. and Sidoroff, F. (1979). Damage Induced Elastic Anisotropy, *Colloque Euromech.*, **115**, Villard de Lans, France.

Dang Van, K. (1993). Macro-micro Approach in High-cycle Multiaxial Fatigue, In: McDowell, D.L. and Ellis, R. (eds), *Advances in Multiaxial Fatigue, ASTM STP 1191*, pp. 120–130, ASTM, Philadelphia, USA.

Davoli, P. (2003). Independance of the Torsional Fatigue Limit Upon a Mean Shear Stress, *Int. J. Fatigue*, **25**: 471–480.

De Los Rios, E.R., Tang, Z. and Miller, K.J. (1984). Short Crack Fatigue Behavior in a Medium Carbon Steel, *Fatigue Fract. Engng. Mater. Struct.*, **7**: 97–108.

Eshelby, J.D. (1957). The Determination of the Elastic Field of an Ellipsoidal Inclusion and Related Problems, *Proc. R. Soc. Lon.*, **A241**: 376–396.

Flaceliere, L. (2004). Contribution à la modélisation du dommage en fatigue multiaxiale d'un acier C36 - confrontation à l'expérience -, In: Doctoral Thesis of University of Poitiers, LMPM/ENSMA, France.

Gros, V. (1996). Etude de l'amorçage et de la propagation des fissures de fatigue dans les essieux-axes ferroviaires, In: Doctoral Thesis of the Central School of Paris, Paris, France.

Hayakawa, K. and Murakami, S. (1998) Space of Damage Conjugate Force and Damage Potential of Elastic-plastic-damage Materials, In: Voyiadjis, G.Z., Ju, J.-W.W. and Chaboche, J.L. (eds), *Damage Mechanics in Engineering Materials*, Elsevier Science BV, London, UK.

Hoshide, T. and Socie, D.F (1987). Mechanics of Mixed Mode Small Fatigue Crack Growth, *Engineering Fracture Mechanics*, **26**: 842–850.

Hoshide, T. and Socie, D.F. (1988). Crack Nucleation and Growth Modeling in Biaxial Fatigue, *Engineering Fracture Mechanics*, **29**(3): 287–299.

Lemaître, J. (1985). A Continuous Damage Mechanics Model for Ductile Fracture, *Journal of Engineering Materials and Technology*, **107**: 83–89.

Lemaître, J. (1992). *A Course on Damage Mechanics*, Springer Verlag.

Maugin, G.A. (1999). *The Thermodynamics of Nonlinear Irreversible Behaviours, An Introduction*, Singapore, World Scientific.

McDowell, D.L. (1999). Damage Mechanics End Metal Fatigue: a Discriminating Perspective, *International Journal of Damage Mechanics*, **8**: 376–403.

Miller, K.J. (1993). Materials Science Perspective of Metal Fatigue Resistance, *Materials Science and Technology*, **9**: 453–462.

Murakami, S. and Kamiya, K. (1997). Constitutive and Damage Evolution Equations of Elastic-brittle Materials based on Irreversible Thermodynamics, *Int. J. Mech. Sci.*, **39**(4): 473–486.

Sauzay, M. (2000). Effets de surface et d'anisotropie en fatigue multiaxiale, In: Doctoral Thesis of Département Génie Mécanique, ENS de Cachan: Paris.

Socie, D.F. (1993). Critical Plane Approaches for Multiaxial Fatigue Damage Assessment, In: McDowell, D.L. and Ellis, R. (eds), *Advances in Multiaxial Fatigue*, ASTM STP 1191, pp. 7–36, A.S.f.T.a. Materials, Philadelphia.

Wei, Y., Chow, C.L., Neilsen, M.K. and Fang, H.E. (2000). Damage Mechanics based Fatigue Life Prediction for 63Sn-37Pb Solder Material, In: *ASME International Mechanical Engineering Congress & Exposition*.

Wei, Y., Chow, C.L., Neilsen, M.K. and Fang, H.E. (2004). Constitutive Model for Sn-Pb Solder under Fatigue Loading, *Int. J. Damage Mech.*, **13**: 147–161.

Yang, X.J. and Chow, C.L. (2003). A Unified Viscoplastic Fatigue Damage Model for 63Sn-37Pb Solder Alloy under Cyclic Stress Control, *Int. J. Damage Mech.*, **12**: 225–243.